ChemComm

FEATURE ARTICLE

View Article Online
View Journal | View Issue

Cite this: *Chem. Commun.*, 2023, **59**, 1728

Recent advances in fluorescence chemosensors for ammonia sensing in the solution and vapor phases

Pandi Raja Lakshmi,†[a] Binduja Mohan,†[a] Preeti Kang,[a] Pandurangan Nanjan*[b] and Sankarasekaran Shanmugaraju*[a]

Developing low-cost and reliable sensor systems for the detection of trace amounts of toxic gases is an important area of research. Ammonia (NH_3) is a commonly produced industrial chemical and a harmful colorless pungent gas released from various manufacturing and processing industries. Continuous exposure to NH_3 vapor causes serious menace to human health, microorganisms, and the ecosystem. Exposure to relatively higher concentrations of NH_3 severely affects the respiratory system and leads to kidney failure, nasal erosion ulcers, and gastrointestinal diseases. Excessive accumulation of NH_3 in the biosphere can cause various metabolic disruptions. As a consequence of this, therefore, suitable sensing methods for selective detection and quantification of trace amounts of NH_3 are of utmost need to protect the environment and living systems. Given this, there have been significant research advances in the preceding years on the development of fluorescence chemosensors for efficient sensing and monitoring of the trace concentration of NH_3 both in solution and vapor phases. This review article highlights several fluorescence chemosensors reported until recently for sensing and quantifying NH_3 in the vapor phase or ammonium ions (NH_4^+) in the solution phase. The wide variety of fluorescence chemosensors discussed in this article are systematically gathered according to their structures, functional properties, and fluorescence sensing properties. Finally, the usefulness and existing challenges of using the fluorescence-based sensing method for NH_3 detection and the future perspective on this research area have also been highlighted.

Received 30th November 2022,
Accepted 9th January 2023

DOI: 10.1039/d2cc06529k

rsc.li/chemcomm

[a] *Department of Chemistry, Indian Institute of Technology Palakkad, Palakkad-678557, Kerala, India. E-mail: shanmugam@iitpkd.ac.in*
[b] *School of Physical Sciences, Amrita Vishwa Vidyapeetham, Mysuru Campus-570026, Karnataka, India. E-mail: pandurangan@my.amrita.edu*
† These authors contributed equally.

Pandi Raja Lakshmi

Dr Pandi Raja Lakshmi obtained her BSc degree in chemistry from Gandhigram Rural Institute, Gandhigram, Dindigul. After this, she completed her MSc and MPhil degrees in chemistry from Mother Teresa Women's University, Kodaikanal. In 2020, she received her PhD in inorganic chemistry from Gandhigram Rural Institute, Gandhigram, Dindigul. She worked as a research assistant at the Indian Institute of Technology Palakkad till March 2022. Her research interest includes mainly developing small-molecule fluorescence sensors for sensing anions, cations, and small molecules.

Binduja Mohan

Ms Binduja Mohan is currently a PhD student at the Indian Institute of Technology Palakkad. She has completed her MSc in chemistry from St. Thomas College Palai and BSc in Chemistry from B K College, Amalagiri. Her research interests are supramolecular self-assembly and sensor chemistry.

Introduction

Designing useful sensor systems for selectively sensing and monitoring the trace concentration of toxic gaseous species is crucial to mitigate environmental pollution and eliminating water, air, and soil pollution.[1] There are many kinds of gas sensors that have already been devised and used for hazardous gas sensing in different areas like ecological investigation, self-propelled manufacturing, therapeutic application, air quality controls, *etc.*[2] The common small molecule gases include CO, NO_X (X = 0.5, 1, and 2), SO_X (X = 2 and 3), and ammonia (NH_3), which are classified as dangerous toxic gases to human health and serious pollutants to the environment when their concentration exceeds the permissible limit of 1 to 5 ppb.[3,4] Among different toxic gases, NH_3 is a prevalent caustic gas in the biosphere and, as it happens, is released from both natural and manufacturing processes.[5] The current global annual production of NH_3 is 176 million tonnes and it is predominantly produced *via* the Haber Bosch process.[6–8] The annual emission of NH_3 gas into the atmosphere is 1.0 Tg.[9] In nature, NH_3 is generated in the nitrogen cycle from decaying organic nitrogen compounds *via* plant decomposition, excretion by humans and animals, and decomposition of sewage by microorganisms.[10–12] NH_3 is artificially produced from agricultural activities, household cleaning products, and industrial processes such as mining, metallurgical activities, production of ceramic materials, and synthesis of various chemical compounds.[13,14]

Due to its intense pungent smell and high sensitivity to the human nose, the smell of NH_3 gas is more easily detected at high concentrations compared to that of other odoriferous gases.[15] However, at a very low concentration, the smell of NH_3 cannot be sensed by the human nose. The permissible limit of dissolved NH_3 is 25 μg L^{-1}; beyond this limit, it is considered toxic.[16] Excess accumulation of NH_3 in the biosphere leads to metabolic disruption and changes in the pH value induced by basicity imbalance of most significant amino acids like lysine and arginine.[17] Continuous exposure to NH_3 vapors leads to kidney disorders, nasal erosion ulcers, and gastrointestinal diseases.[18] Therefore, developing suitable sensor systems for selective sensing and monitoring of the trace concentration of NH_3 in the gas phase or NH_4^+ in the solution phase is urgently needed. Numerous instrumentation techniques, including flow spectroscopy, gas chromatography–mass spectrometry (GC–MS), potentiometric electrodes, infra-red absorption, and spectrophotometry, and a few reaction-based sensing methods like Nessler's reagent test and Berthelot reaction are currently available for the detection and quantification of NH_3.[19–22] Another sensing technology currently used is electrochemical sensing of NH_3. The electrochemical sensing method is highly sensitive and relatively cheap.[23]

Nonetheless, the above instrumentation techniques devour chemicals, need illustration pre-treatment, affluent instrumentation, have high instrument cost, and are not suitable for on-site real-time monitoring, which limits their practical use for continuous monitoring of the concentration of NH_3 gas.[24,25]

Preeti Kang

Ms Preeti Kang is currently a PhD student at the Indian Institute of Technology Jodhpur, India. She received her MSc degree in chemistry from the Indian Institute of Technology Palakkad, Kerala, India in 2021. Her research work is on fabricating new catalytic systems for biofuels and fine chemicals and fluorescence sensor design.

Pandurangan Nanjan

Dr Pandurangan Nanjan obtained his MSc in chemistry from Periyar University, Tamil Nadu, India, in 2006. After that, he worked in the industry from 2006 to 2009 and then joined Amrita University, Kerala, India, in 2009 as a PhD scholar. His PhD thesis work was on natural product isolation, characterization, synthesis, and biological activities. In 2018, he moved to the Indian Institute of Technology Palakkad, India, as an institute post-doctoral fellow. Presently, he is working at Amrita Vishwa Vidyapeetham, Amrita University, as a Senior Assistant Professor in the science department. His research interests include natural products, synthetic polymers, and medicinal chemistry.

Sankarasekaran Shanmugaraju

Dr Sankarasekaran Shanmugaraju received his BSc and MSc degrees in chemistry from The American College, Madurai, and his PhD degree with a gold medal for the best thesis in inorganic chemistry from the Indian Institute of Science (IISc), Bengaluru. In 2014, he moved to Trinity College Dublin, Ireland, as an Irish Research Council (IRC) postdoctoral fellow. Since October 2018, he has been an assistant professor at the Indian Institute of Technology Palakkad. His current research activities are in the area of supramolecular materials and sensor chemistry.

The reaction-based colorimetric sensing method often gives false positive results due to other interfering contaminants that co-exist in the samples.[26] Moreover, many of the available sensor systems function only at high temperatures to stimulate the adsorption and desorption of NH_3, which further restricts their room-temperature practical applications.[27] To circumvent these drawbacks, in recent years, optical method-based detection has become an efficient and practically feasible method for sensing NH_3 gas under ambient conditions. In particular, fluorescence-based sensing methods have garnered substantial research interest because of their technical simplicity, fast response time, low instrument cost, and high sensitivity for detection.[28,29] Fluorescence-based sensing is a powerful method that can be used to detect the target analytes with superior sensitivity.[30]

Until recently, a plethora of fluorescence chemosensors like luminescent metal–organic frameworks, metal–organic hybrid gels, porous organic polymers, and small-molecule fluorescence sensors including the ratiometric fluorescence sensors have been developed and demonstrated for their fluorescence sensing applications towards NH_3.[31–35] Several of these sensors exhibit high selectivity, good sensitivity, and excellent reversibility for NH_3 detection. A few review articles have already been reported on fluorescence chemosensors for detecting toxic gaseous molecules.[36–38] However, to the best of our knowledge, until now, no dedicated review articles have been reported that exclusively elaborate on fluorescence chemosensors for NH_3 sensing. Given this, in this review article, we have systematically described various fluorescence chemosensors reported to date for the selective detection and quantification of NH_3 both in the solution and vapor phases. For the understanding purpose, we categorized the fluorescence chemosensors into several types, (i) metal–organic framework (MOF)-based chemosensors, (ii) metal–organic gel (MOG)-based chemosensors, (iii) covalent-organic polymer (COP)-based chemosensors, and (iv) small-molecule fluorescence chemosensors. In the following sections, each categorized fluorescence chemosensor design, synthesis, structure features, photophysical characteristics, and NH_3 sensing properties have been discussed in detail.

Metal–organic framework (MOF)-based fluorescence chemosensors

Metal–organic frameworks (MOFs) are an emerging class of highly ordered porous polymeric networks built through metal–ligand coordination bonding between metal ions or metal clusters and multidentate organic ligands.[39] In general, MOFs are isolated as highly crystalline solids after heating suitable organic ligands with metal ions in a stoichiometric molar ratio in an appropriate solvent.[40] Owing to the large surface areas, high porosity, and tailorable structures and functional properties, the application of MOFs has been explored in great detail for gas adsorption and storage, host–guest chemistry, heterogeneous catalysis, chemosensing, stimuli-responsive

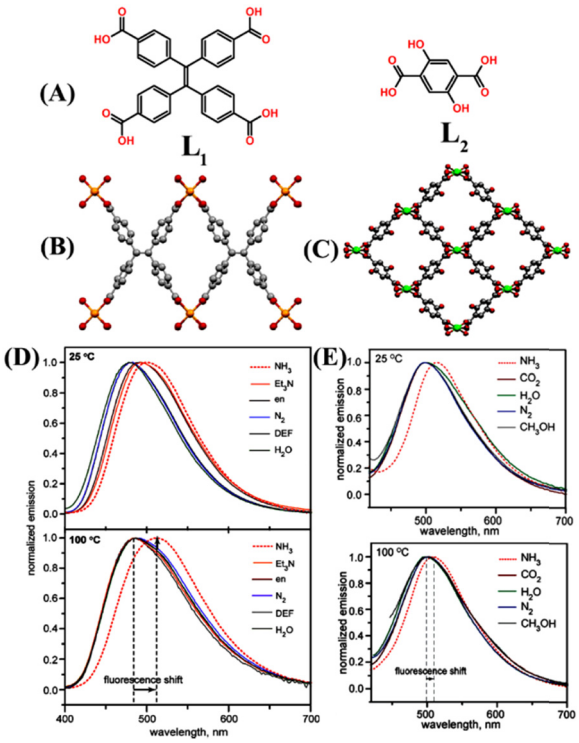

Fig. 1 (A) Molecular structure of ligands L_1 and L_2. X-ray crystal structure of (B) LMOF **1** and (C) LMOF **2** (colour code: Zn orange, Mg green, O red, and C gray). Hydrogen atoms are not included for clarity. The relative changes in emission spectra of (D) **1** and (E) **2** when exposed to different analytes at 25 °C (top) and 100 °C (bottom). Reprinted with permission from ref. 47. Copyright 2013 American Chemical Society.

drug delivery and so on.[41–43] In particular, in the preceding years, luminescent metal–organic frameworks (LMOFs) have attracted considerable research focus because of their interesting, tunable photophysical properties.[44,45] LMOFs have been used for various applications such as optical materials, luminescent chemosensors, adsorptive sensing and removal of pollutants, targeted drug delivery, and diagnostic bioprobes.[46] In this section the design, structural features, and NH_3 sensing properties of various LMOFs reported to date have been discussed.

Two microporous LMOFs, Zn_2(TCPE) (**1**) and Mg(H_2DHBDC) (**2**) {where TCPE = tetrakis(4-carboxyphenyl)ethylene (L_1) and $H_2DHBDC_2^-$ = 2,5-dihydroxybenzene-1,4-dicarboxylate (L_2)} were specially designed for the 'turn-on' fluorescence sensing of gaseous NH_3 at high temperatures (Fig. 1(A)–(E)).[47] The synthesized LMOFs exhibited high structural rigidity and strong fluorescence emission properties. Both LMOFs **1** and **2** exhibited selective 'turn-on' fluorescence sensing responses when they were exposed to gaseous NH_3 at 100 °C. The fluorescence enhancement was accompanied by a significant red shift in the emission maxima from λ = 487 nm to 511 nm (Fig. 1(D) and (E)). Interestingly, similar exposure studies of these LMOFs to other potentially interfering analytes such as water, methanol, larger amines, ethylenediamine (en), and *N*,*N*′-dimethylformamide (DMF) showed no strong binding

affinity at higher temperatures. However, at 25 °C, these analytes elicited a notable shift of 0 to 23 nm in the emission maxima. Moreover, LMOF **1** on binding with NH_3 induced an irreversible phase change and, thus, is not suitable for reversible fluorescence sensing applications, while thermally activated LMOF **2** reversibly interacted with NH_3 gas. The possible binding mode of NH_3 with LMOFs was probed using density-functional theory (DFT) calculations. The calculated binding energies for NH_3 were high and were more favorable for binding NH_3 by 19 to 38 kJ mol^{-1} than other tested analytes, which makes the LMOFs highly selective for NH_3 sensing. The unique chemical selectivity of LMOFs for NH_3 over other interfering analytes was ascribed to the small pore sizes, which is preferred for the selective uptake (molecular sieving effect) of NH_3 vapor due to matching of their complementary size with the micropores of LMOFs. These studies demonstrated that temperature could be used as a feasible external stimulus to enhance the chemical selectivity in chemical sensing applications, and this parameter can further be extended for the selective sensing of other hazardous environmental pollutants and contaminants.

A robust microporous Mg-based LMOF **3** was designed incorporating active hydroquinone into an Mg-LMOF, $\{[(CH_3)_2NH_2][Mg_3(OH)(DHBDC)_3(TPP)]_n\}$ (SNNU-88, SNNU = Shaanxi Normal University, 2,5-dihydroxyterephthalic acid (DHBDC) = $\mathbf{L_3}$, 2,4,6-tri(4-pyridyl)-pyridine, TPP = $\mathbf{L_4}$) and used for effective detection of NH_3 at trace concentration (5 to 100 ppm) (Fig. 2(A)).[48] The idea of incorporating hydroquinone is that it can serve dual functions, *i.e.*, redox behavior and proton transfer. Furthermore, hydroquinone also serves as an excellent molecular recognition site for the NH_3 analyte. The ligand $\mathbf{L_3}$ is a versatile organic chelator that forms porous networks upon reactions with metal ions or metal clusters and exhibits keto to enol tautomerism, further extending the framework stability of the synthesized LMOF **3**. Upon diffusion of NH_3 vapors to the surface of LMOF **3**, they will react with the hydroquinone groups through acid–base interactions that promote the transformation of enol to the keto form. The adsorbed NH_3 would accept a proton from hydroquinone and form an ammonium ion (NH_4^+), and effused electrons reduce the LMOF resistance. At the same time, during the recovery process, the loss of H^+ ions from NH_4^+ accelerates the reverse transformation of keto to the enol form, increasing the resistance of LMOF. Furthermore, the addition of aqueous NH_3 into a dimethylacetamide (DMA) solution of **3** showed a strong fluorescence emission (Fig. 2(B)). It was observed that the emission intensity decreased as the concentration of aqueous NH_3 increased from 0 to 1.5 ppm, and a further increase in aqueous NH_3 concentrations from 3 to 100 ppm resulted in a significant enhancement in emission intensity with an apparent red-shift of 35 nm at room temperature (Fig. 2(C) and (D)). The observed unusual fluorescence 'turn-off' to 'turn-on' sensing properties of **3** originated from an excited state intramolecular proton transfer (ESIPT) mechanism.[48] The addition of NH_3 destroys the intramolecular hydrogen bonding in hydroquinone and promotes a strong intermolecular hydrogen bonding between hydroquinone and

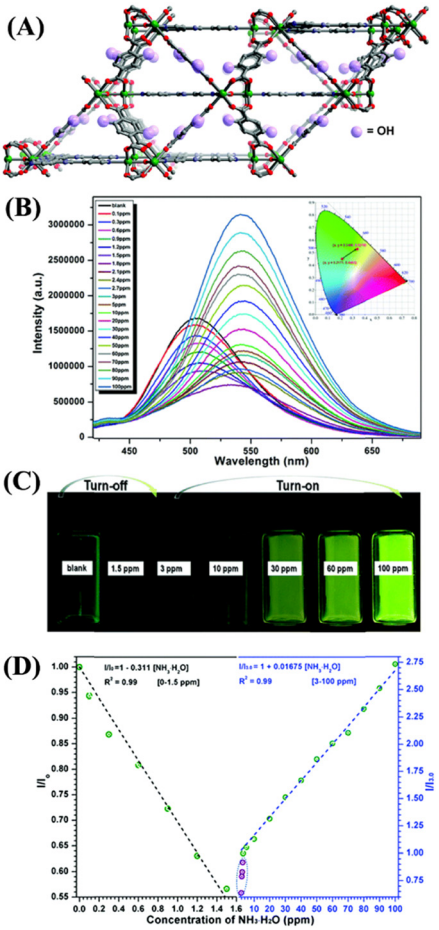

Fig. 2 (A) 3D framework structure of LMOF **3**. (B) Relative changes in fluorescence intensity of **3** upon increasing aqueous NH_3 concentration from 0 to 100 ppm in DMA medium. (C) Photographs for the turn-off and turn-on fluorescence behavior triggered by aqueous NH_3. (D) Linear relationship between the observed efficiency of fluorescence changes and the aqueous NH_3 concentration was recorded in DMA. Reprinted with permission from ref. 48. Copyright 2018 Royal Society of Chemistry.

NH_3 molecules. Interestingly, the ESIPT-based sensing of NH_3 is highly reversible; thus, LMOF **3** can be a good reusable sensor for NH_3 sensing. The high selectivity, ultra-trace sensitivity, and good reversibility make LMOF **3** a powerful chemosensor for sensing NH_3.

Very recently, Cui *et al.* reported three anionic LMOFs **4–6**, $\{[Zn_3(BTEC)_2(H_2O)(4\text{-BCBPY})]\cdot(H_2O)\}_n$ {where $BTEC^{4-}$ = 1,2,4,5-benzene tetracarboxylic acid anion ($\mathbf{L_5}$), 4-$BCBPY^{2+}$ = 1,1′-bis(4-cyanobenzyl)-4,4′-bipyridinium dication ($\mathbf{L_6}$)} (Fig. 3(A)–(C), left).[49] LMOFs **4–6** were synthesized by solvothermal heating using different metal salts ($ZnNO_3$ for **4**, $ZnCl_2$ for **5**, and $ZnSO_4$ for **6**), and these LMOFs were structurally characterized by X-ray diffraction analysis which revealed that each MOF structure is built from binuclear metal building units, which are coordinatively connected to two protonated $BTEC^{4-}$ ligands and three Zn(II) ions. The extended structures of LMOFs results in the formation of a porous channel that acts as a host to accommodate the guest, 4-$BCBPY^{2+}$ cyano-viologen, into it to achieve charge balance. LMOFs **4–6** showed good photosensitivity on

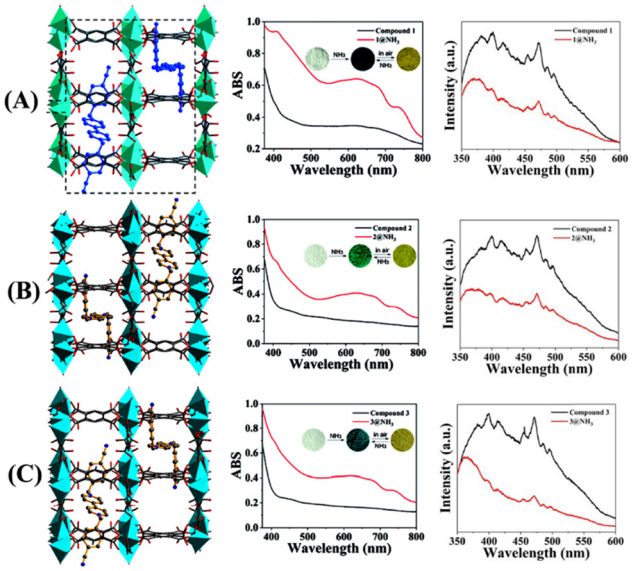

Fig. 3 3D packing structure of LMOFs (A) **4**, (B) **5**, and (C) **6** (left); changes in UV-vis absorption (middle; inset: discoloration photographs for reversible adsorption and desorption of NH_3), and fluorescence emission change (right) before and after exposure of **4–6** to NH_3 vapor. Reprinted with permission from ref. 49. Copyright 2022 Royal Society of Chemistry.

exposure to sunlight and UV light and had high thermal stability up to ~400 °C. In addition, these LMOFs displayed visible color changes upon exposure to NH_3 vapors (Fig. 3(A)–(C), right). The initial color of LMOFs changed from white to blue, and further exposure to air reversibly changed the color from blue to gray, which could be seen through naked eye. These photochromic changes were attributed to the distinct differences in donor–acceptor (D–A) distances and π–π stacking distances in three LMOFs due to the different natures of metal salts. Further studies confirmed that LMOFs **4–6** could sense NH_3 vapors at a very trace concentration through a fluorescence quenching mechanism. Upon irradiation, the efficient transfer of electrons from NH_3 to electron-poor viologen guest caused the observed fluorescence quenching. These studies demonstrated that the judicious selection of metal salts, organic linkers, and the choice of appropriate guest molecules could help modulate photochromic properties and detection of NH_3 vapor.

An interesting 2,1,3-benzoxadiazole decorated electron-deficient Zr(IV)-based LMOF 7 for 'turn-on' fluorescence sensing of NH_3 was recently reported by the Potapov group.[50] LMOF 7 was prepared by heating a mixture of a dicarboxylate ligand, 4,7-di(*p*-carboxyphenyl)-2,1,3-benzoxadiazole ($\mathbf{L_7}$), and zirconium tetrachloride in DMF (Fig. 4(A)). After prolonged heating, the framework structure of 7 was isolated in quantitative yield. LMOF 7 belongs to the UIO-68 family with fcu topology and a very high surface area (Fig. 4(A)). The photophysical studies of 7 in H_2O showed a broad absorption peak with absorption maxima at λ = 380 nm and a strong emission peak centered at λ = 530 nm, which was red-shifted by 20 nm compared to ligand $\mathbf{L_7}$ peak due to the influence of ligand-to-metal coordination interactions within the framework (Fig. 4(B)).

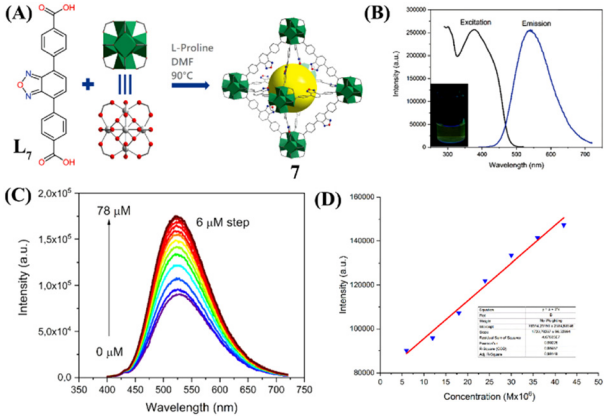

Fig. 4 (A) Synthesis of sensor LMOF **7** from ligand $\mathbf{L_7}$ and Zr(IV); (B) Excitation and emission spectra of **7** were measured in H_2O (inset: photographs of **7** in H_2O); (C) Changes in fluorescence emission intensity for **7** upon the gradual addition of aqueous NH_3. (D) Linear fit for the NH_3 concentration–intensity correlation. Reprinted with permission from ref. 51. Copyright 2022 Royal Society of Chemistry.

The photoluminescence quantum yield was determined to be 35%, which is significantly higher compared to the quantum yield of the ligand $\mathbf{L_7}$ alone. To use it for NH_3 sensing, a well-dispersed suspension of 7 was prepared in H_2O and subsequently treated with NH_3 in an aqueous medium. The initial emission intensity of 7 drastically increased after adding aqueous NH_3. From the titration profile, the limit of detection (LoD) for NH_3 was determined to be 6.5 ppb which is much superior to those of the well-known Nessler's reagent and many of the LMOFs reported for NH_3 sensing (Fig. 4(C) and (D)). To meet the practical applicability, the 'turn-on' fluorescence sensing property of 7 was also demonstrated using a filter-paper-based test strip for vapor phase sensing of NH_3. The experimentally observed 'turn-on' fluorescence sensing was further validated by DFT calculation on the model system of 7, explaining the reason for the observed increase in fluorescence intensity upon adding NH_3. It was proposed that the addition of electron-rich NH_3 to the electron-deficient 7 perturbed the symmetry of the electron density distribution and resulted in an excited state charge separation, consequently increasing the fluorescence emission intensity. In a nutshell, these studies demonstrated the relevance of Zr(IV) based LMOFs for their applications in sensing and quantifying toxic gases in an aqueous medium.

Metal–organic gel (MOG)-based fluorescence chemosensors

The fabrication of metal–organic gel (MOG)-based responsive soft materials is a fast-growing area of research in supramolecular chemistry.[51] MOGs are formed *via* non-covalent supramolecular self-assembly of discrete metal–organic constructs into highly cross-linked and intertwined three-dimensional (3D) networks. Commonly, the voids in the 3D framework of MOGs are filled with a large volume of solvent molecules.

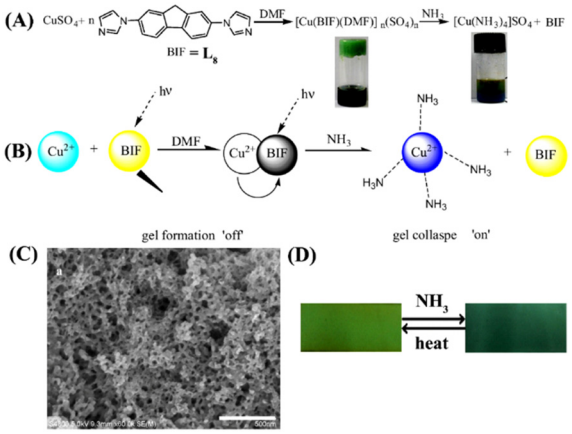

Fig. 5 (A) Reaction scheme for forming **8** and depolymerization after exposure to NH_3 vapor (inset: visual color change from green gel to purple) and (B) corresponding proposed sensing mechanism of gel formation and collapse on sensing NH_3 vapor. (C) SEM image of the as-synthesized **8** and (D) reversible sensing responses showed instinct color changes upon exposure to NH_3 and subsequent heating of the gel-coated sheet. Reprinted with permission from ref. 53. Copyright 2016 Elsevier.

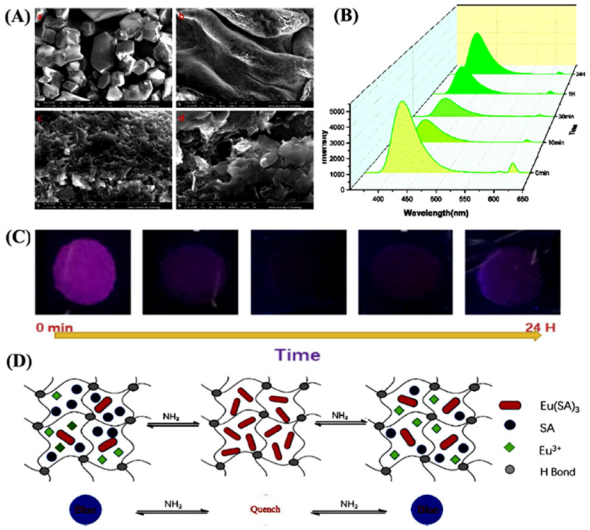

Fig. 6 (A) SEM images (scale: 1–5 μM) of Eu(Sal)$_3$-Fm/PVA hydrogel (**10**). (B) Fluorescence emission spectrum of **10** in response to 5 mmol concentrations of NH_3. (C) Photographs of hydrogel **10** exposed to NH_3 gas for about 0 min to 24 h; the images were taken under 254 nm UV lamp illumination. (D) Schematic representation for the proposed sensing mechanism of NH_3 sensing through complexation and decomplexation processes. Reprinted with permission from ref. 54. Copyright 2021 Elsevier.

Among the wide variety of MOGs, reported in recent years, luminescent MOGs (LMOGs) have attracted increasing attention because of their applications as chemical sensors for the detection of environmental pollutants.[52] In this section, we have highlighted some noteworthy examples of LMOG-based fluorescence chemosensors for detecting NH_3.

In 2016, Zhou *et al.* introduced a new idea of designing chemical sensors for NH_3 sensing *via* gel formation, which collapse upon binding with the analyte.[53] The team developed a fluorescent and colorimetric probe for NH_3 sensing using a Cu(II)-based LMOG **8**. Sensor **8** was synthesized by reacting 2,7-bis(1-imidazole)fluorene (**L$_8$**) with $CuSO_4$ (Fig. 5(A)). A green color solution was observed instantaneously by stirring a mixture of ligand **L$_8$** and $CuSO_4$ in DMF and after 5 minutes of stirring, the solution transformed into a highly opaque green gel **8**. Scanning electron microscopy (SEM) images of the formed gel showed a clear fibrous network-like structure (Fig. 5(C)). Interestingly, upon exposure of **8** to the saturated NH_3 vapors showed a remarkable fluorescence 'turn-off' and 'turn-on'-type of chemosensing due to the collapse of gel, and the LOD was calculated to be up to 5 ppm (Fig. 5(B) and (D)). The initial green color of the gel transformed to purple due to the depolymerization of the metal–ligand coordination polymer. The depolymerization drives the replacement of ligand **L$_8$** from the coordination sphere of **8**, which results in tetragonal $[Cu(NH_3)_4]^{2+}$ formation. The LMOG **8** showed highly selective fluorescence responses for NH_3 as well as for ethylenediamine, while other organic amines and solvents showed no noticeable changes in the emission properties. Furthermore, the sensing responses were found to be reversible and the gel was stable for up to five cycles of sensing studies. These studies confirm that LMOG **8** can be a potential fluorescent chemosensor for the sensitive, selective, and reversible detection of NH_3 vapors.

Last year, a novel lanthanide complex-based luminescent hydrogel **9** was synthesized from the reaction of $EuCl_3{\cdot}6H_2O$ and salicylic acid (Sal, **L$_9$**).[54] The synthesized gel **9** showed an effective sensing ability for NH_3 vapor under optimum conditions. Furthermore, the EuL_n-Fm/PVA hydrogel (**10**) which is composed of Eu(Sal)$_3$ and Eu(TTA)$_3$ complexes (PVA = polyvinyl alcohol, TTA = 2-thenoyltrifluoroacetone (**L$_{10}$**), L = Sal, or TTA, and Fm = formamide, n = 1–3) was obtained in a one-pot reaction and **10** was used for the continuous monitoring of NH_3 gas (Fig. 6). Interestingly, the fluorescence sensing response was not affected by the presence of any other interferences from external sources (Fig. 6(B)). The binding of NH_3 with the Eu(Sal)$_3$ complex influences the energy transfer from the ligand to metal ions and thus evokes changes in the fluorescence emission intensity. Although the increasing concentration of NH_3 decomposes the coordination complex and destabilizes it, the intrinsic fluorescence of **9** is quenched and recovered by adjusting the concentration of NH_3. The ability of Eu(Sal)$_3$ to show unique fluorescence responses was attributed to its effective coordination with NH_3 gas. Considering the facile preparation and cost-effectiveness, both LMOG **9** and **10** can be realized as potential chemosensor systems for the effective sensing and monitoring of NH_3 gas under optimum conditions.

Covalent-organic polymer (COP)-based fluorescent chemosensors

Covalent organic polymers (COPs) are a new class of solid materials that have attracted increasing research interest and

have been used as promising luminescent materials for sensing hazardous and environmentally toxic pollutants.[55] Generally, COPs are synthesized *via* conventional covalent bond-forming reactions between appropriate organic building units.[56] Due to their high specific surface area, low framework density, and high physicochemical stability, COPs have been widely used for the analysis and quantification of trace amounts of toxic small molecules.[57–62] In this section, we have discussed three luminescent COP-based fluorescent chemosensors for NH_3 sensing.

In 2018, Zhang *et al.* designed and synthesized a novel triazine-based covalent organic polymer **11** for the sensitive detection of HCl and NH_3 vapors.[63] The COP **11** was isolated as a yellow powder by heating 2,4,6-trimethyl-1,3,5-triazine ($\mathbf{L_{11}}$) and 1,4-terephthalaldehyde ($\mathbf{L_{12}}$) in methanol at 80 °C (Fig. 7(A)). The powder form of **11** was dispersed in a solvent-medium and the microporous film formed by it on the surface of the quartz sheets exhibited high selectivity and sensitivity for HCl and NH_3 vapor sensing (Fig. 7(B) and (C)). Using the dispersed powder of **11** in an HCl-bubbled solvent medium diminished the initial fluorescence intensity of the polymer, along with a notable red shift in the emission maxima. This red shift was ascribed to the protonation-induced charge-transfer transition.

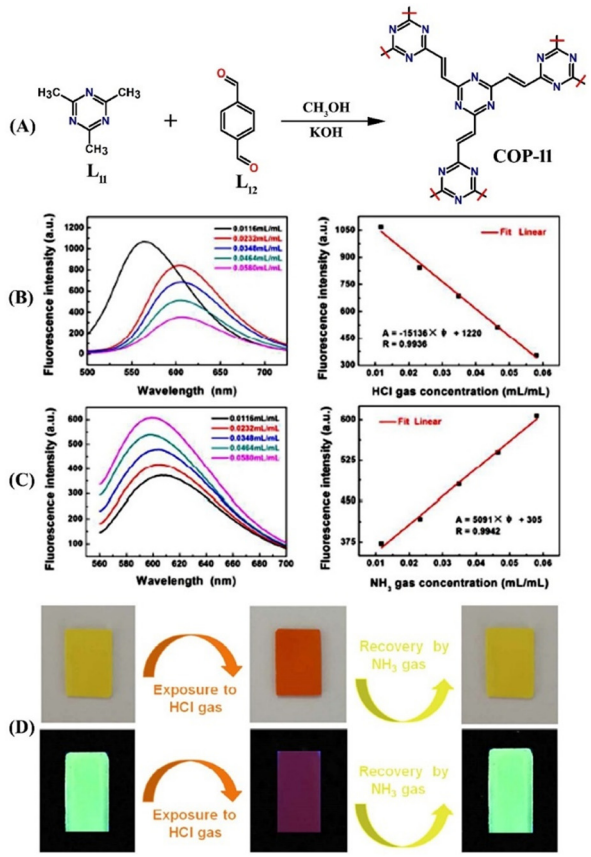

Fig. 7 (A) Schematic representation for the synthesis of COP **11**. (B) Fluorescence quenching responses of the films formed by **11** on exposure to HCl gas at various concentrations (left) and linear relationship of changes in fluorescence intensities as a function of the various concentration of HCl gas (right). (C) Fluorescence quenching responses of the films formed by **11** on exposure to NH_3 gas at various concentrations (left) and linear relationship of changes in fluorescence intensities as a function of the various concentration of NH_3 gas (right). (D) Photographs for visual color changes of the films formed by **11** under visible light (top) and a UV lamp (bottom) before and after exposure to HCl gas and subsequent fluorescent recovery by NH_3 gas exposure. Reprinted with permission from ref. 63. Copyright 2018 Royal Society of Chemistry.

Interestingly, the subsequent injection of NH_3 led to the reappearance of fluorescence emission due to the deprotonation in a basic medium. Additionally, the micropores on the film's surface were substantial for excellent sensing of gaseous small molecules like NH_3 and HCl. The film showed similar fluorescence 'on-off' sensing responses to HCl and NH_3. Gratifyingly, **11** displayed marked visual color changes from green to orange upon exposure to HCl. The initial color was visible again due to the deprotonation by NH_3 vapor (Fig. 7(D)). Similar color changes were also observed for a freshly prepared microporous film. Computational calculations further validated the proposed protonation and deprotonation-based sensing mechanism. The detection limit for HCl gas was determined to be 1.0967×10^{-4} mL mL^{-1}; for NH_3 gas, it was calculated to be 5.8925×10^{-4} mL mL^{-1}. Furthermore, COP **11** selectively binds with HCl in the presence of other toxic gases like SO_2, CO_2, benzene, *etc.* The fluorescence sensing responses were found to be reversible, and no reduction in the initial emission intensity was observed even after several cycles of sensing studies. These results demonstrate that COP **11** can be considered a potential fluorescence chemosensor for quantitative detection and continuous monitoring of the concentration of HCl and NH_3 gases.

Organic cross-linked acrylic ester-based organic polymer microparticles (**12**) embedded with different fluorescent dyes such as fluorescein and acridine orange, were fabricated and successfully used as a 'turn-on' fluorescence chemosensor for sensitive and selective detection of NH_3 and concentrations of various organic amines.[64] The fluorescein-doped microparticles **12** showed a fast response time, reversible sensing, and a low detection limit of 0.73 ppm for NH_3 detection. Similarly, various organic amines also interact with fluorescein-doped **12** particles in the following order: triethylamine > *tert*-butylamine > diethylamine > *n*-propylamine > NH_3. The interaction between the **12** microparticles and fluorescein dye was mainly hydrogen-bonding and hydrophobic interactions. Due to the facile protonation and neutral environment, organic particles **12** exhibited a weak fluorescence emission and after adding NH_3 or amine vapors; the deprotonation reactions enhance the fluorescence intensity and this 'turn-on' fluorescence is not affected by the humidity. Owing to the facile fabrication and excellent fluorescence sensing responses, the organic polymer-based microparticles **12** are practically good candidates for detecting and monitoring the concentrations of NH_3 and organic amines.[64]

In general, covalent organic frameworks and crystalline organic polymers are non-emissive due to the occurrence of the π–π layer stacked aggregation-caused fluorescence quenching (ACQ) phenomenon which thus limits their practical applications as fluorescence sensors. To overcome this limitation,

Jiang *et al.* developed a general synthetic strategy to design highly emissive covalent organic frameworks by introducing aggregation-induced emission (AIE) active fluorophores.[65] The well-known AIE fluorophore tetraphenyl ethylene (TPE, tetraphenylethylene-tetraboronic acid, $\mathbf{L_{13}}$) was used to design a highly emissive covalent organic framework **13**. Compound **13** was readily synthesized by reacting ligands $\mathbf{L_{13}}$ and 1,2,4,5-tetrahydroxy benzene ($\mathbf{L_{14}}$) in a 1 : 1 molar ratio in a mixture of dioxane/mesitylene after heating at 90 °C for 3 days (Fig. 8(A) and (B)). The SEM imaging of **13** demonstrated its rectangular belt-shaped morphology and it was found to be highly emissive when imaged under a fluorescence microscope (Fig. 8(C) and (D)). **13** showed an absorption band at λ = 390 nm and a strong solid-state emission peak at λ = 500 nm with an absolute fluorescence quantum yield of 32%. **13** was reported to have 2 to 3 times more fluorescence emission compared to the TPE model compound and this enhanced fluorescence emission confirms the additional contribution emanating from π–π intermolecular layers and restriction of free molecular rotation. It was conceived that due to the presence of a boronate–ester linkage in which boronate acts as a Lewis acid and forms an acid–base adduct with NH_3 gas which acts as a Lewis base, **13** exhibits enhanced NH_3 uptake through adduct formation. As anticipated, indeed, **13** exhibited a rapid fluorescence sensing response towards NH_3. As shown in Fig. 8(E), the initial strong fluorescence emission of **13** (2 mg in 2 mL of toluene) was drastically quenched upon the gradual addition of NH_3.

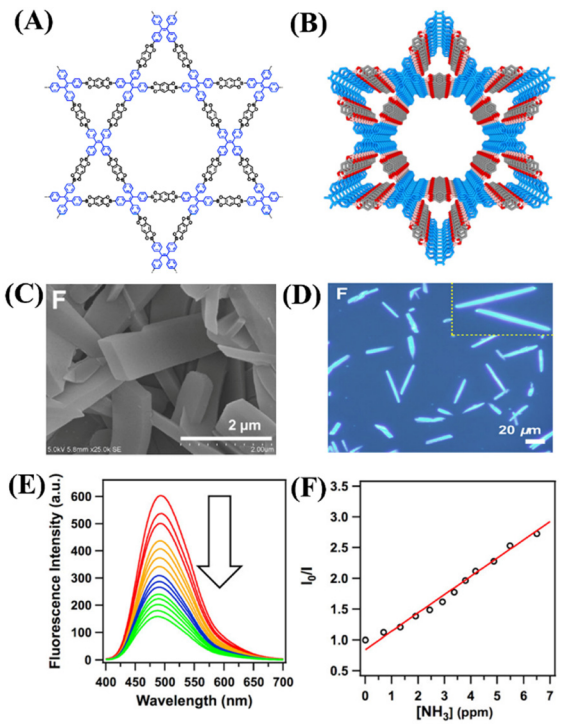

Fig. 8 (A) and (B) Framework structure of COP **13**. (C) and (D) FE-SEM and fluorescence microscopy images of **13**. (E) Observed fluorescence quenching for **13** in toluene upon the addition of NH_3 and (F) corresponding Stern–Volmer plot. Reprinted with permission from ref. 65. Copyright 2016 American Chemical Society.

A linear Stern–Volmer plot was obtained from the titration data and the fluorescence quenching rate constant ($K_q = K_{SV}/\tau$) was calculated to be 4.1×10^{14} M^{-1} S^{-1} (Fig. 8(F)). This extremely high value indicated that **13** is highly sensitive and can sense NH_3 at as low as sub-ppm level concentration. This new synthetic strategy is useful for the design of highly emissive porous, crystalline organic polymers and for exploring their fluorescence sensing applications for the analysis of trace amounts of hazardous and toxic pollutants.

Small-molecule-based fluorescence chemosensors

In recent years, small-molecule fluorophores have become attractive fluorescence chemical sensors for selective sensing of targeted analytes.[66] The facile synthesis, easy purification, and comfortable chemical modifications empower the small molecule-based fluorescence sensors as a potential alternative to the polymer-based sensor systems.[66,67] In contrast to the polymeric sensors, the high solubility in common solvents and enhanced solution processability benefit the small-molecule fluorescence sensors in practical applications. Furthermore, facile synthesis and functional group modification help in making small-molecule sensors more selective for a particular type of targeted analytes. Among the wide variety of small-molecule fluorophores, boradiazaindacenes dyes (BODIPY) have been used extensively as fluorescent chemosensors for the detection of various analytes. Until recently, the BODIPY dyes have created huge interest in the field of sensor chemistry because of their interesting, tunable photophysical properties, chemical inertness, strong absorption, and emission in the visible region.[68,69] Several BODIPY dye-based fluorescence chemosensors have been designed and successfully employed for the detection of trace amounts of toxic gases including NH_3. In this section, we have exemplified notable small-molecule-based fluorescence chemosensors for NH_3 detection.

In 2011, Shen and co-workers designed a novel aza-BODIPY small molecule sensor **14**, which was functionalized with two fused pyrazine rings and successfully used as a colorimetric and fluorometric sensor for selective sensing of ammonium (NH_4^+) ions (Fig. 9(A)).[70] The two pyrazine rings were introduced with the intention that the tetrahedral structure of NH_4^+ could form multiple hydrogen bonds with pyrazine-N as well as with N at the *meso* position of BODIPY dye. Interestingly, the UV-visible absorption titration of **14** with various metal cations such as Zn(II), Cd(II), Hg(II), Co(II), Fe(III), Fe(II), Ni(II), Mn(II), Cu(II), Mg(II), Na(I), Al(III), and Ca(II) showed no detectable changes in the absorption intensity. However, similar titration studies using NH_4^+ cations exhibited significant changes in the absorption spectrum of **14** (Fig. 9(B), left). The high selectivity of sensor **14** toward NH_4^+ ions compared to other metal cations was attributed to the ability to form four N–H hydrogen bonds. The original absorption intensity of free **14** decreased considerably and a new weak broader band appeared at λ = 505 nm upon the increasing addition of ammonium acetate in THF

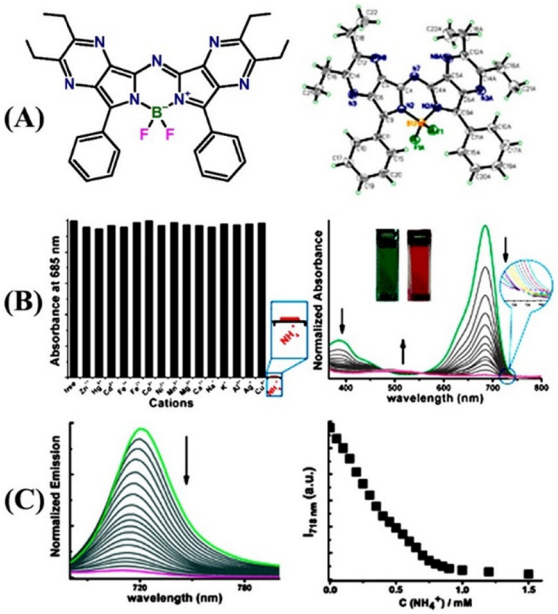

Fig. 9 (A) Structure of sensor **14** (left) and its X-ray crystal structure (right). (B) Relative changes in absorption intensity for **14** upon the addition of various metal ions and NH_4^+ ion (left) and relative changes in the absorption spectrum of **14** upon increasing the concentration of ammonium acetate (right, the inset shows the observed color changes before and after the addition of NH_4^+ ions). (C) Observed changes in fluorescence emission intensity of **14** with increasing concentration of NH_4^+ ions (left) and a plot of changes in emission intensity at λ = 718 nm for the increasing concentration of NH_4^+ ions (right). Reprinted with permission from ref. 70. Copyright 2011 Royal Society of Chemistry.

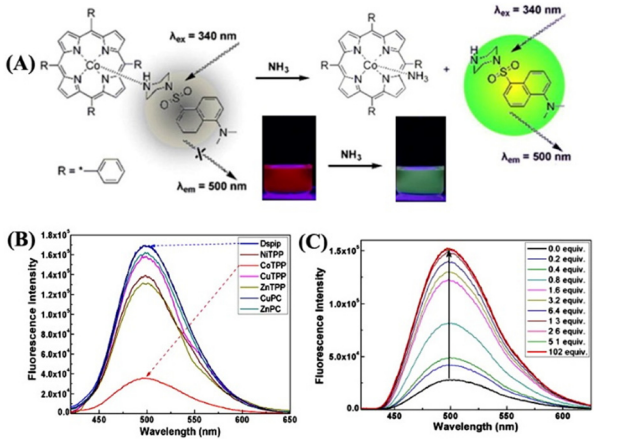

Fig. 10 (A) Proposed sensing mechanism for the fluorescence enhancement of [Co(TPP)(Ds-pip)] complex (**15**) upon the addition of NH_3 (inset: sharp visual color changes before and after the addition of NH_3). (B) Observed fluorescence responses of the dansylpiperazine fluorophore binding with different metal porphyrin complexes in DCM solution. (C) Enhanced emission intensity of **15** upon the addition of NH_3 in the DCM solution. Reprinted with permission from ref. 71. Copyright 2011 Elsevier.

solution (Fig. 9(B), right). These notable changes in absorption intensity were further reflected in the obvious visual color changes of **14** from green to red-pink before and after the addition of NH_4^+ ions, respectively, which enabled the detection of NH_4^+ ions in solution through naked eye. The observed blue shift in the absorption intensity and sharp-visual color changes are due to the typical H-aggregate formation *via* hydrogen-bonding interactions with NH_4^+ ions in the solution. The H-aggregate formation causes significant fluorescence quenching and the molar absorptivity co-efficient diminishes upon increasing the NH_4^+ ion concentration. The strong emission band of **14** at λ = 718 nm quenched drastically in with increasing NH_4^+ ion concentration (Fig. 9(C)). The fluorescence quenching upon the H-aggregate formation occurs due to either the non-radiative decay being the dominant pathway or promotion of intersystem crossing to the triplet state. These studies demonstrated that BODIPY dye-based sensor **14** can be a potential fluorescence and colorimetric sensor for the detection of NH_3 as NH_4^+ ions in solution.

A novel porphyrin-based Co(II) metal complex [Co(TPP)(Ds-pip)] {**15**; TPP = tetraphenyl porphyrin ($\mathbf{L_{15}}$); DS-pip = dansylpiperazine ($\mathbf{L_{16}}$)} substituted with a dansyl fluorophore has been judiciously designed and employed as a turn-on fluorescence chemosensor for the detection and quantification of NH_3.[71] The well-known displacement approach was adopted to develop the 'turn-on' fluorescence sensor **15**. The dansylpiperazine fluorophore $\mathbf{L_{16}}$ occupies the axial position and coordinates with Co(II) metal through the piperazine-N atom. Due to the occurrence of a photoinduced intramolecular electron-transfer (PET) process, the complex [Co(TPP)(Ds-pip)] is weekly emissive. However, exposure to NH_3 gas replaced the coordinated $\mathbf{L_{16}}$ fluorophore from the axial position, which resulted in an enhanced fluorescence emission due to the inhibition of PET processes (Fig. 10(A)). The fluorescence enhancement was also reflected from the sharp visual color changes. It was also demonstrated that among various metal porphyrin complexes, only the [Co(II)TPP] complex was found to be strongly bound with the dansylpiperazine fluorophore, and hence the changes in fluorescence emission intensity depend on the ionophore units (Fig. 10(B)). The displacement of the fluorophore by NH_3 took place through non-covalent bonding interactions. There are several advantages of using non-covalent interactions in sensor chemistry: (i) no tedious synthetic effort is required to link an indicator with a receptor; (ii) considerable freedom in the choice of an appropriate indicator; and (iii) signal transduction is induced by the simple addition of an analyte to the receptor–indicator mixture.

Recently, Flood and co-workers demonstrated ion pair binding studies.[72] Similarly, Smith *et al.* also reported alkali metal ion-pair formation through the ion-pair mechanism.[73] The similar ionic radius of NH_4^+ (286 pm) and K^+ (266 pm) poses challenges in the discrimination of these two cations and designing a sensor that can strongly bind with a high preference for NH_4^+ ions over K^+ is challenging and difficult. To surmount this issue, Kavallieratos *et al.* developed 1,3,5-trimethyl benzene-based two fluorescence sensors, tris-(3,5-dimethyl)-pyrazole (**16**) and tris(3,5-diphenyl)pyrazole (**17**), for selective detection of NH_4^+ through the ion-pair mechanism (Fig. 11(A)).[74] Sensor **16** exhibited noticeable fluorescence

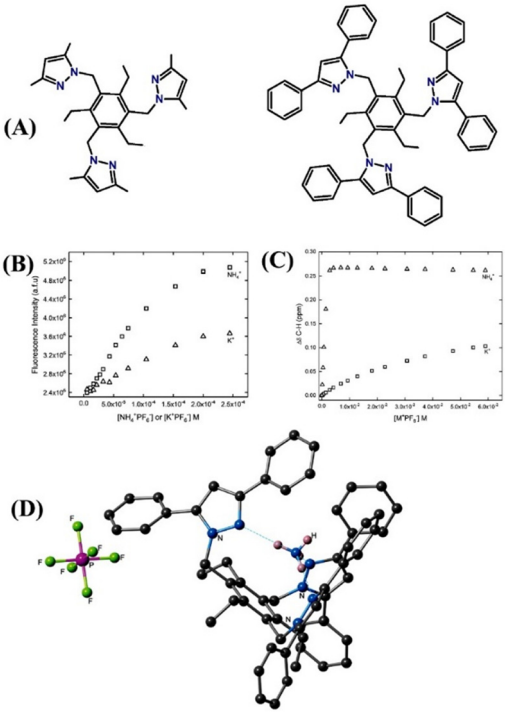

Fig. 11 (A) Structure of sensors **16** (left) and **17** (right). (B) Fluorescence titration studies of **16** with NH_4^+ and K^+ ions were recorded in CH_3CN/CH_2Cl_2. (C) ^1H NMR titration plot of **16** (2 mM) with NH_4^+ and K^+ was recorded in acetone-d_6. (D) X-ray crystal structure of [**17** + NH_4^+] + PF_6 shows the hydrogen bonding between NH_4^+ and sensor **17**. Reprinted with permission from ref. 74. Copyright 2017 Royal Society of Chemistry.

enhancement on increasing the concentration of NH_3, while sensor **17** showed almost negligible fluorescent enhancement (Fig. 11(B)). These striking differences in fluorescence responses confirm the role of dimethyl and diphenyl groups attached to the core of the sensor systems. Furthermore, the ^1H NMR studies indicated a 1 : 1 complexation between sensors and ions, and the association constant K_a was calculated to be 74 000 ($\pm$900) M^{-1} for **16**·NH_4^+ and 22 ($\pm$1) M^{-1} for **16**·K^+ formation (Fig. 11(C)). The higher K_a value establishes the preferential binding affinity of **16** for NH_4^+ ions over K^+ ions. In the solid state, **17** binds more strongly with NH_4^+ ions than sensor **16**; this is due to the multiple hydrogen bonding interactions as it is shown in the X-ray crystal structure of the host–guest complex (Fig. 11(D)). These experimental results were validated by DFT calculation, which explained the strong ion-pair complexation between sensors and NH_4^+ ions. These studies demonstrate the importance of substituents in the pyrazole moiety in dictating the analyte binding strength and selectivity.

Ingo and co-workers introduced a novel fluoroionophore mechanism of sensing NH_3.[75] The sensor **18**-based membrane consists of an NH_4^+ ion-sensitive fluoroionophore physically entrapped within a hydrophilic polyurethane hydrogel with the help of an internal buffer solution. The membrane gets covered with a hydrophobic and gas-permeable protective layer that acts as a proton and ion barrier to prevent any interaction of the sensitive layer with charged species. The sensing mechanism

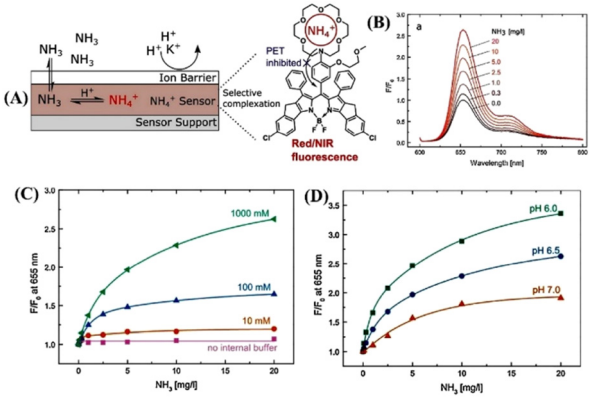

Fig. 12 (A) New fluoroionophore mechanism for sensing of NH_4^+ ions. (B) Changes in fluorescence emission spectra of the sensor **18** membrane were measured at different NH_3 concentrations. (C) Calibration curves of the sensing materials with different buffer capacities. (D) Calibration curves of sensor **18** with different pH values of the internal buffer. Reprinted with permission from ref. 75. Copyright 2018 Elsevier.

involves the diffusion of NH_3 across the protective membrane inside the sensor, where NH_3 is protonated by a low pH buffer and is converted to NH_4^+ ions. The recognition unit, aza-crown ether present in **18**, effectively and reversibly binds the NH_4^+ ions (Fig. 12(A)). In the absence of NH_3, the lone pairs on the nitrogen of the aza-crown ether cause an intramolecular fluorescence quenching caused by the PET transition. The fluorescence of the indicator is enhanced when the NH_4^+ analyte is complexed; it interacts with the nitrogen lone pair of the aza-crown ether, which results in inhibition of the PET process (Fig. 12(A) and(B)). An aza-18-crown-6 moiety was chosen as a receptor since the dimensions of the crown ether cavity excellently match the size of the NH_4^+ ions. A π-extended rigid BODIPY dye was chosen as an indicator molecule because of its interesting and tunable photophysical properties. Furthermore, the sensor membrane can bind with NH_3 at different internal buffer concentrations as well as at various pH values of the sensor medium (Fig. 12(C) and (D)). The changes in pH did not significantly influence the overall sensing efficiency of the sensor. This new method of fluoroionophore sensing can further be extended for the selective detection of various analytes by selecting appropriate aza-crown ether receptor units.

The supramolecular self-assembly process is a powerful method to generate intricate supramolecular architectures and functional structures and materials. The pre-programmed building units, under the influence of external stimulus, can self-assemble into structures and materials of varied morphology and functional properties.[76] The properties of self-assembled structures highly depend on the morphological outcome and this can be modulated by employing an external stimulus. The π-conjugated organic building units are known to form stacked self-assembly structures and it has been demonstrated that solvent plays an important role in controlling the morphological outcome due to the solvent–solute interactions which greatly affect the self-assembly processes.[51]

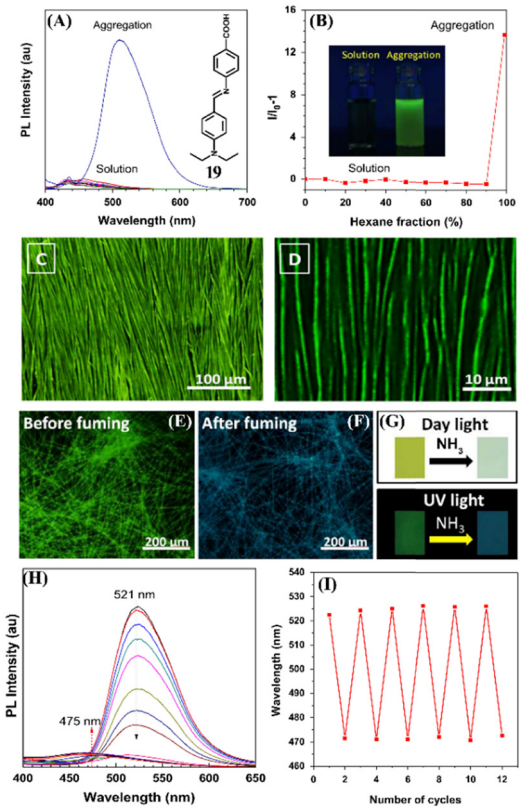

Fig. 13 (A) Photoluminescence spectra of **19** in THF solution and aggregates were formed in the THF–hexane mixture (inset: structure of **19**). (B) A plot of hexane fraction *vs* relative changes in emission intensity (inset: photographs of solution and aggregates of **19**). (C) and (D) Fluorescence microscopy images of the self-assembled structure of **19** under different magnifications. (E)–(G) Color changes were observed before and after fuming NH_3. (H) Changes in fluorescence emission intensity of **19** after the addition of NH_3. (I) Reversible fluorescence sensing responses of **19** under heating and fuming conditions. Reprinted with permission from ref. 77. Copyright 2016 Elsevier.

In light of this, Han *et al.* reported solvent-directed self-assembly formation of long-order fluorescent filaments based on a Schiff base organic ligand, **19**, (*E*)-4-(((4-(diethylamino)-benzylidene)amino)benzoic acid) (DBBA).[77] Ligand **19** displayed both aggregation-induced emission (AIE) and twisted intramolecular charge-transfer transition (TICT) which makes **19** highly fluorescent and consequently it can be used as an effective fluorescent sensor for NH_3 sensing (Fig. 13(A) and (B)). By simply tuning the dewetting process, a long-order filament-like organic nanostructure was developed and the self-assembled structure was found to be highly emissive (Fig. 13(C) and (D)). The self-assembled structure of **19** displayed a highly sensitive, fast, and reversible fluorescence sensing response towards NH_3 (Fig. 13(H) and (I)). The higher sensitivity of self-assembled structures in comparison to that of the discrete fluorophore **19** was ascribed to the long-range electronic communication. These studies demonstrated the advantages of self-assembly processes to devise suitable sensing platforms for reversible and sensitive detection and quantification of toxic gases.

In recent years, the design and use of small-molecule-based ratiometric fluorescence probes has become an important area of research, and they have been demonstrated to be an excellent sensing platform compared to the traditional ways of sensing analytes concerning the environment and biology.[78] It has been studied that the use of conventional fluorescence sensing methods for particular analytes with high selectivity is often difficult and, in some cases, the fluorescent probes failed to exhibit high selectivity. However, this can be surmounted by ratiometric fluorescence sensing because a high selectivity can be realized by placing the indicator and reactive functional groups at the right places through the judicious selection of appropriate fluorescent probes and reactive units.[79]

In 2008, Mayr and co-workers fabricated an interesting fluorescence sensing system employing cellulose ester nanospheres incorporated with small-molecule fluorescent dye eosin ethyl ester (**20**) and 2′,7′-dichlorofluorescein methyl ester (**21**) which acts as a fluorescent indicator for monitoring of trace amounts of dissolved NH_3 at sub-mg L^{-1} levels (Fig. 14(A)).[80] Fluorescent indicators **20–21** interacts strongly with NH_3 through ($-H_3N$: ↔ H–O–) acid–base adduct formation (Fig. 14(B)). The presence of the ester group on indicator dyes facilitates their dissolution and well-dispersion within the cellulose ester polymer matrix and thus prevents leaching. The NH_3-sensitive layer (sensing membrane) was covered with a silicone layer to make it low cross-sensitive towards pH changes. In practical application in seawater and freshwater, the covered silicon layer blocks the proton transfer to the pH indicator, and the sensor membrane responds to ultra-fast detection of NH_3 approximately within 30 minutes of contact time. Additionally, the fluorescence response was found to be reversible and the sensing membrane could easily be reproduced for subsequent sensing cycles. The detection limit was estimated to be around μg L^{-1}.

Borisov *et al.* developed highly photostable and sensitive fluorescence sensors based on aza-BODIPY dyes for monitoring the concentrations of NH_3.[81] The aza-BODIPY dyes **22** and **23** were selected as fluorescence indicators because of their low pK_a values of 4.4 and 3.9, respectively (Fig. 14(C)). The sensors

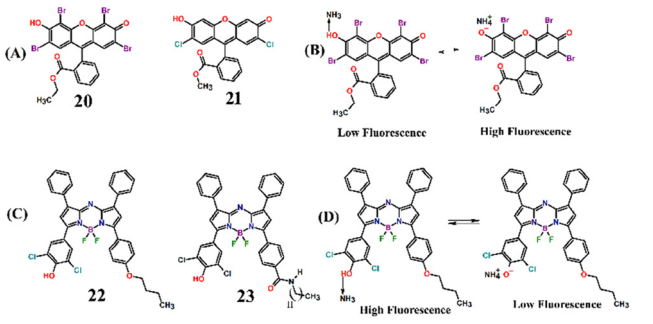

Fig. 14 (A) Molecular structure of fluorescent indicator dyes **20** and **21** and (B) their proposed fluorescence sensing mechanism of detection of NH_3 through acid–base equilibrium. (C) Molecular structure of aza-BODIPY sensors **22** and **23** and (D) their proposed fluorescence sensing mechanism of detection of NH_3 through acid–base equilibrium.

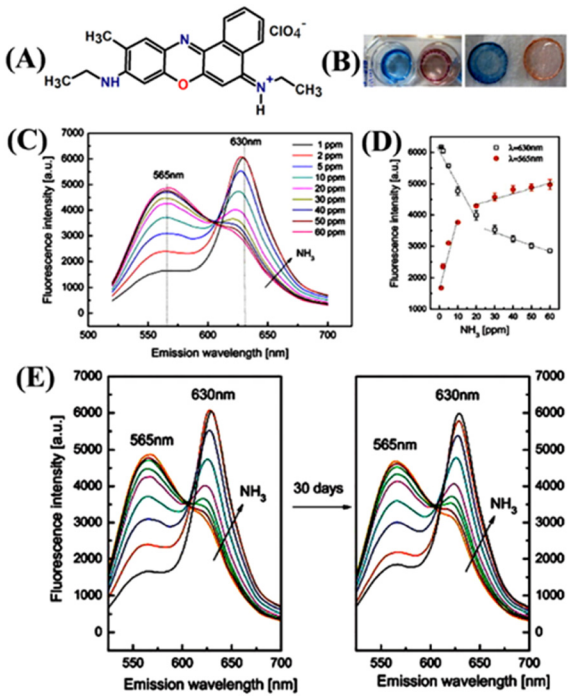

Fig. 15 (A) Structure of ratiometric fluorescence dye **24**. (B) Color changes were observed for the **24**-based sensing membrane before (left) and after the exposure to NH_3. (C) Ratiometric fluorescence responses were observed to various concentrations of NH_3 (1–60 ppm) in water. (D) Calibration curves were measured at emission wavelengths of 565 nm and 630 nm upon NH_3 exposure. (E) Time-dependent stability study in presence of NH_3 in the range of 1–60 ppm. Reprinted with permission from ref. 82. Copyright 2014 Elsevier.

22 and **23** were physically entrapped within hydrogels and then dispersed in silicone rubber. Furthermore, this layer was covered with a hydrophobic Teflon membrane, which acts as an additional proton barrier and light scattering layer. The NIR-emitting Egyptian blue dye was used as a reference and changes in fluorescence properties were recorded using a compact phase fluorometer. The aza-BODIPY dyes sense NH_3 through an acid–base equilibrium sensing mechanism (Fig. 14(D)). The two –Cl atoms at the *ortho*-position to phenolic OH induce the electron-withdrawing effect making the dye strongly acidic. It was found that the lower the pK_a value of the dye, the higher the sensitivity of the sensors. Before the binding of NH_3, the aza-BODIPY dyes were highly emissive and the fluorescence intensity was quenched upon formation of an acid–base complex with NH_3. The deprotonated dyes possess efficient photoinduced electron transfer, which quenches the intrinsic fluorescence of dye-based sensors. By carefully tuning the ratio between dyes and hydrogel matrix, a high sensitivity of 0.11–300 μg L^{-1} was achieved for NH_3 detection. Therefore, the aza-BODIPY dye-based ratiometric fluorescence sensors possess high potential for their practical applications such as monitoring NH_3 concentrations in fish farming and wastewater monitoring, *etc.*

An oxazine 170 perchlorate fluorescent dye **24** was conveniently used as a ratiometric fluorescence sensor for the monitoring of trace concentration of NH_3 in water (Fig. 15(A) and (B)).[82] Furthermore, an effective sensing thin film membrane was fabricated by mixing **24** with ethyl cellulose and this sensing membrane exhibited numerous characteristics like high selectivity for detection, good reversibility, fast-sensing responses, resistance to alkalinity, less photo-bleaching, and long-term stability. Considering these interesting properties, Rhee and co-workers devised a thin-film sensing membrane by blending **24** dyes with ethyl cellulose and successfully used it for the appropriate sensing of dissolved NH_3 in water. The sensing membrane was found to be stable in different pH ranges from 5.5 to 11 and no great variation in the emission spectra of the membrane was observed. However, upon the addition of NH_3, the fluorescence emission intensity was drastically enhanced and a new band appeared at λ = 565 nm, which was ascribed to the dissociative reaction of NH_3 in H_2O as shown below (Fig. 15(C)).

$$NH_3 + H_2O \rightarrow NH_4^+OH^-$$

$$NH_4^+OH^- + H^+Dye^- \rightarrow NH_4^+Dye^- + H_2O$$

$$NH_4^+Dye^- \leftrightarrow H^+Dye^- + NH_3$$

The ratio between the initial emission maxima at λ = 630 nm and the new peak at λ = 565 nm after NH_3 addition led to the design of a ratiometric sensor. Furthermore, the ratiometric assessment explained the maximum NH_3 concentration that can be detected in artificial wastewater which is 1–50 ppm (Fig. 15(D) and (E)). The proposed thin-film membrane-based ratiometric sensing probe is a cost-effective, easily adaptable,

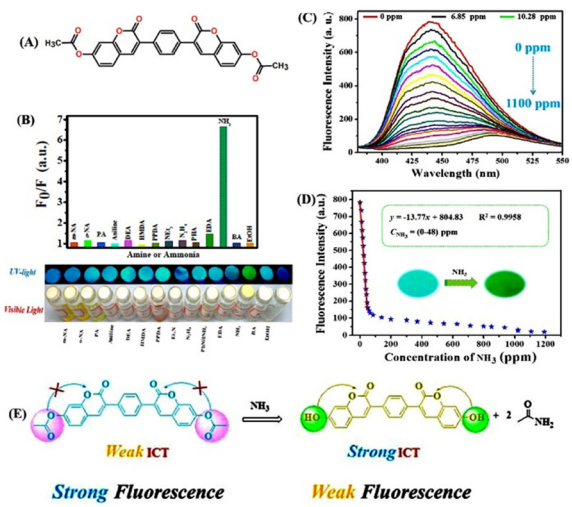

Fig. 16 (A) Structure of ratiometric fluorescence dye **25**. (B) Observed relative changes in emission intensity of the as-prepared sensor **25** when it was exposed to various amines, ammonia, and ethanol. (C) Emission spectra of the paper-based sensor when it was exposed to different concentrations of NH_3 vapor. (D) Linear fitting analysis for the changes in emission intensity *versus* the concentration of NH_3 vapor (inset: photographs of the sensor before and after exposure to NH_3 vapor taken under 365 nm UV light). (D) Proposed reaction-based fluorescence sensing mechanism. Reprinted with permission from ref. 83. Copyright 2020 Royal Society of Chemistry.

Table 1 Summary of fluorescence sensing properties of various sensors **1–25** discussed in this article

Sensor	λ_{em} (nm)	Quantum yield (Φ)/life-time (τ)	Sensing phase/analyte	Selectivity for NH_3 or NH_4^+/other analyte(s)	Sensing mechanism	Reversibility	Response time	Measurable concentration range	Ref.
1	487	—	Vapor/NH_3	High/—	Zn–NH_3 coordination	Irreversible	—	—	47
2	500	—	Vapor/NH_3	High/—	Mg–NH_3 coordination	Reversible	—	—	47
3	505	—	Liquid/$NH_3{\cdot}H_2O$	High/—	ESIPT	Reversible	87 s	0–1.5 ppm (turn-off) 3–100 ppm (turn-on)	48
			Vapor/NH_3	High/—	Semiconductor NH_3 sensing			5–100 ppm	48
4–6	404–405	—	Vapor/NH_3	High/$Cr_2O_7^{2-}$	Intermolecular electron transfer	Reversible	3–15 s	—	49
7	530	0.35/6–7 ns	H_2O/aq·NH_3	High/aliphatic amines	Excited state charge separation	Reversible	—	6.5 ppm	50
8	560	—	Vapor/NH_3	High/ethylene diamine	Gel collapse *via* depolymerization	Reversible	<5 s	5 ppm	53
9	421, 619	—	Vapor/NH_3	High/—	Gel collapse *via* NH_3 coordination	Reversible	—	mM	54
10	421, 619	—	Vapor/NH_3				0.1 ms		
11	453	0.52/—	Vapor/NH_3	High/HCl	Deprotonation	Reversible	—	5.89×10^{-4} mL mL^{-1}	63
12	528	0.039/—	Vapor/NH_3	High/organic amines	Deprotonation	Reversible	<1 s	0.73 ppm	64
13	500	0.32/0.7 ns	Vapors/NH_3	High/—	Lewis acid–base pair formation	—	Rapid response	sub-ppm	65
14	721	—	Liquid/NH_4^+	High/metal-cations	H-aggregate formations	—	—	mM	70
15	500	—	Vapor/NH_3	High/—	Inhibition of the PET process	—	—	40 nM	71
16	298	—	Liquid/NH_4^+	High/—	Ion-pair mechanism	—	—	mM	74
17	335	—	Liquid/NH_4^+	High/—	Ion-pair mechanism	—	—	mM	74
18	655	0.68/—	Buffer/NH_4^+	High/—	Inhibition of PET	Reversible	60 s	36 μg L^{-1}	75
19	535	6.72/—	Fumed/NH_3	High/—	TICT	Reversible	Rapid response	35 mM	77
20	536	0.5/—	Liquid/NH_4^+	High/—	Acid–base equilibrium	Reversible	min	μg L^{-1}	80
21	522	0.9/—	Liquid/NH_4^+	High/—	Acid–base equilibrium	Reversible	min	μg L^{-1}	80
22	725	—	Buffer/NH_4^+	High/—	Acid–base equilibrium and PET	Stable adduct (irreversible)	Long-response time	μg L^{-1}	81
23	725	—	Buffer/NH_4^+	High/—	Acid–base equilibrium and PET	Stable adduct (irreversible)	Long-response time	μg L^{-1}	81
24	565, 630	—	Liquid/NH_4^+	High/—	Deprotonation	Reversible	10 s	ppm	82
25	445		Vapour NH_3	High/organic amines	Strong ICT	—	Ultra-fast	0.71 ppm	83

and convenient method for multiple uses of monitoring NH_3 concentration in H_2O.

A novel bi-coumarin-based fluorescent probe, 7,7′-(acetoxy)-3,3′-(*p*-phenylene)bis(coumarin) (**25**), was designed for sensitive detection of various amines and ammonia both in solution and air (Fig. 16).[83] Sensor **25** was synthesized using the Perkin reaction between 1,4-phenylenediacetic acid and 2,4-dihydroxybenzaldehyde. In **25**, the acetyl group is a reactive site that efficiently reacts with amine or NH_3. Initially, **25** exhibited a strong fluorescence emission at λ = 445 nm due to the weak ICT-based electronic transition, which was quenched upon the addition of different amines {diethylamine (DEA), hexamethylenediamine (HMDA), ethylenediamine (EDA), benzylamine (BA)} and NH_3 (Fig. 16(A) and (B)). The fluorescence quenching (~97.4%) was accompanied by appearance of a new weak fluorescence emission peak at λ = 500 nm (Fig. 16(C)). The addition of amines or NH_3, which act as a nucleophile to cleave the methoxycarbonyl groups on **25** to generate OH groups enhances the ICT-transition efficiency because of the strong electron-donating ability of OH groups (Fig. 16(E)). The proposed sensing mechanism was validated by ^{1}H NMR titration studies and DFT calculations. A marked visual color change from bright blue to yellow was observed after fuming with NH_3 vapor and this instant visual color change makes **25** a potential reaction-based fluorescent sensor for real-time monitoring of the NH_3 concentrations in spoiled food samples.

Conclusions and outlook

Ammonia (NH_3) is a toxic gas that poses a serious threat to human health and causes pollution in the environment. The widespread use of NH_3 in manufacturing and processing industries has led to an increase in its concentrations in the atmosphere and often the concentration level goes beyond the permissible level. Therefore, until recently, a plethora of fluorescent chemosensors have been carefully designed for monitoring the trace concentration of NH_3 both in solution and vapor phases. In this review article, we have systematically highlighted the synthesis, photophysical, and fluorescence sensing properties of a wide variety of fluorescent chemosensors for NH_3 detection. The fluorescent sensors (**1–25**) discussed in this article are grouped according to their structural features and functional properties. Table 1 summarizes the fluorescence sensing properties of all the sensors discussed herein. Gratifyingly, many of the chemosensors exemplified in this article exhibited rapid fluorescence sensing response time, an ultra-trace detection limit, excellent chemical stability, and high selectivity toward the detection of NH_3. More importantly, a few of them have been fabricated as miniaturized portable sensing devices and they have been successfully demonstrated for the efficient detection of NH_3 gas.

The polymer-based fluorescence sensors (MOFs, MOGs, and POPs) exhibited good sensitivity for the detection of ultra-trace amounts of NH_3 because of the long-range electronic communication along the polymer chain. However, polymer-based fluorescence sensors lack solution processability due to their poor solubility in common solvents, which limits their practical film-based sensing applications. The high solubility, facile synthesis, and good solution processability engendered the small-molecule-based fluorescence sensors as a reliable and alternative sensing platform for device fabrication to monitor NH_3 concentration in real-time. Furthermore, the reaction-based fluorescence sensors have been demonstrated to exhibit high sensing selectivity for NH_3 detection. Although, a large number of fluorescence sensors have been developed and used for NH_3 sensing, developing practically feasible suitable fluorescence sensors with superior sensitivity and selectivity for sensing and quantifying the ultra-trace concentrations of NH_3 is still required. There are several drawbacks in each kind of fluorescence sensor known to date for realizing their practical applications. The polymer-based fluorescence sensors have been largely exploited in sensor chemistry, but their poor chemical, air, and hydrolytic stability is a bottleneck for their practical applications. The chemical stability of polymers can be addressed and improved by physically entrapping them within a stable matrix that acts as a membrane to enhance stability and prevent polymer decomposition. Also, it has been demonstrated that in some cases there exists a lack of high selectivity with polymer-based sensor systems, and this can be overcome by attaching targeted or reactive functional groups to the polymer skeletons. Some of the polymer-based fluorescence gas sensors are quite large and very expensive and thus, in recent years, using small-molecule-based fluorescence sensors have become a convenient sensing method for the detection of NH_3.

Despite several advantages of small molecule-based fluorescence sensors, their poor sensitivity for detection is a major hindrance. The sensitivity of small-molecule sensors can be improved by linking them either covalently or non-covalently. Therefore, small-molecule sensors can be viewed as lead compounds for further developing practically feasible potential fluorescence sensors. Similarly, the reaction-based fluorescence sensors have become a topical area of research because of their excellent selectivity for detection, and less interference from other competing analytes. However, since it involves a chemical reaction between sensors and analytes, their fluorescence sensing responses are high but not useful for fast sensing applications. Furthermore, the ratiometric sensors lack reusability and using them is not a cost-efficient method for detection. These disadvantages may be addressed by introducing reactive functional groups within the polymeric network or embedding the ratiometric probes within the polymeric matrixes, in which the long-range sensing communication can enhance the fluorescence sensing response time and additionally, heterogeneity of polymers helps to achieve recyclability.

In summary, in this review article, we presented a detailed discussion on various aspects of NH_3 sensing and systematically highlighted the recent advances in the design of fluorescence chemosensors for efficient sensing of NH_3 both in solution and vapor phases. We predict that the field of optical sensor chemistry will continue to expand and innovative

sensing technologies will emerge to address the existing challenges of devise fabrication, sensing selectivity, sensitivity, and practical feasibility for on-site real-time detection of toxic gases. We are currently focusing on developing low-cost sensing systems with excellent sensing performances for the selective detection and quantification of small-molecule-based toxic gases. We believe that this review will highly benefit the readers working in the area of sensor chemistry, supramolecular chemistry, and closely related interdisciplinary areas of research.

Conflicts of interest

There are no conflicts to declare.

Acknowledgements

The authors thankfully acknowledge the Science and Engineering Research Board (EMEQ Award EEQ/2018/000799 to SS) for financial support.

References

1 S. Shanmugaraju and P. S. Mukherjee, *Chem. Commun.*, 2015, **51**, 16014–16032.
2 N. Tamaekong, C. Liewhiran, A. Wisitsoraat and S. Phanichphant, *Sensors*, 2010, **10**, 7863–7873.
3 A. Fuerte, R. X. Valenzuela, M. J. Escudero and L. Daza, *J. Power Sources*, 2009, **192**, 170–174.
4 R. Ali, R. F. M. Elshaarawy and S. M. Saleh, *J. Environ. Chem. Eng.*, 2017, **5**, 4813–4818.
5 K. P. Shrestha, L. Seidel, T. Zeuch and F. Mauss, *Energy Fuels*, 2018, **32**, 10202–10217.
6 J. L. M. Hurtado and C. R. Lowe, *ACS Appl. Mater. Interfaces*, 2014, **6**, 8903–8908.
7 T. Abel, B. Ungerböck, I. Klimant and T. Mayr, *Chem. Cent. J.*, 2012, **6**, 1–9.
8 S. Z. Andersen, V. Čolić, S. Yang, J. A. Schwalbe, A. C. Nielander, J. M. McEnaney, K. Enemark-Rasmussen, J. G. Baker, A. R. Singh and B. A. Rohr, *Nature*, 2019, **570**, 504–508.
9 S. N. Behera, M. Sharma, V. P. Aneja and R. Balasubramanian, *Environ. Sci. Pollut. Res.*, 2013, **20**, 8092–8131.
10 S. Biring, A. S. Sadhu and M. Deb, *Sensors*, 2019, **19**, 5124.
11 S. W. M. O. Damink, N. E. P. Deutz, C. H. C. Dejong, P. B. Soeters and R. Jalan, *Neurochem. Int.*, 2002, **41**, 177–188.
12 B. I. Cohen, *Med. Hypotheses*, 2002, **59**, 757–758.
13 L. Peng, X. Yang, L. Yuan, L. Wang, E. Zhao, F. Tian and Y. Liu, *Opt. Commun.*, 2011, **284**, 4810–4814.
14 S. V. Krupa, *Environ. Pollut.*, 2003, **124**, 179–221.
15 A. A. Vaughan, M. G. Baron and R. Narayanaswamy, *Anal. Commun.*, 1996, **33**, 393–396.
16 D. Zhang, J. Zhang, H. Shi, X. Guo, Y. Guo, R. Zhang and B. Yuan, *Sens. Actuators, B*, 2015, **221**, 224–229.
17 M. E. Meyerhoff, Y. M. Fraticelli, J. A. Greenberg, J. Rosen, S. J. Parks and W. N. Opdycke, *Clin. Chem.*, 1982, **28**, 1973–1978.
18 R. Claps, F. V. Englich, D. P. Leleux, D. Richter, F. K. Tittel and R. F. Curl, *Appl. Opt.*, 2001, **40**, 4387–4394.
19 J.-L. Su, B. L. Schumacher, K. M. Lindley, V. Soloveychik, W. Burkhart, J. A. Triantafillou, K. Kuettner and T. Schmid, *Hybridoma*, 2001, **20**, 149–157.
20 A. Daridon, M. Sequeira, G. Pennarun-Thomas, H. Dirac, J. P. Krog, P. Gravesen, J. Lichtenberg, D. Diamond, E. Verpoorte and N. F. de Rooij, *Sens. Actuators, B*, 2001, **76**, 235–243.
21 K. Crowley, A. Morrin, A. Hernandez, E. O'Malley, P. G. Whitten, G. G. Wallace, M. R. Smyth and A. J. Killard, *Talanta*, 2008, **77**, 710–717.
22 D. Li, Z. Li, C. Wang, T. Wang and X. Xu, *IOPScience*, 2019, **4**, 4–13.
23 J. F. M. Oudenhoven, W. Knoben and R. van Schaijk, *Procedia Eng.*, 2015, **120**, 983–986.
24 C. Liu, H. Tai, P. Zhang, Z. Yuan, X. Du, G. Xie and Y. Jiang, *Sens. Actuators, B*, 2018, **261**, 587–597.
25 J. Wang, Z. Li, S. Zhang, S. Yan, B. Cao, Z. Wang and Y. Fu, *Sens. Actuators, B*, 2018, **255**, 862–870.
26 C. J. Chang, T. D. James, E. J. New and B. Z. Tang, *Acc. Chem. Res.*, 2020, **53**, 1.
27 D. Wu, L. Chen, Q. Xu, X. Chen and J. Yoon, *Acc. Chem. Res.*, 2019, **52**, 2158–2168.
28 T. Gorai, W. Schmitt and T. Gunnlaugsson, *Dalton Trans.*, 2021, **50**, 770–784.
29 S. Shanmugaraju, D. Umadevi, L. M. González-Barcia, J. M. Delente, K. Byrne, W. Schmitt, G. W. Watson and T. Gunnlaugsson, *Chem. Commun.*, 2019, **55**, 12140–12143.
30 S. Erbas-Cakmak, S. Kolemen, A. C. Sedgwick, T. Gunnlaugsson, T. D. James, J. Yoon and E. U. Akkaya, *Chem. Soc. Rev.*, 2018, **47**, 2228–2248.
31 S. Shanmugaraju, C. Dabadie, K. Byrne, A. J. Savyasachi, D. Umadevi, W. Schmitt, J. A. Kitchen and T. Gunnlaugsson, *Chem. Sci.*, 2017, **8**, 1535–1546.
32 V. M. Suresh, S. Chatterjee, R. Modak, V. Tiwari, A. B. Patel, T. K. Kundu and T. K. Maji, *J. Phys. Chem. C*, 2014, **118**, 12241–12249.
33 S. Pramanik, C. Zheng, X. Zhang, T. J. Emge and J. Li, *J. Am. Chem. Soc.*, 2011, **133**, 4153–4155.
34 C. Zhang, Y. Che, Z. Zhang, X. Yang and L. Zang, *Chem. Commun.*, 2011, **47**, 2336–2338.
35 G. Das, B. P. Biswal, S. Kandambeth, V. Venkatesh, G. Kaur, M. Addicoat, T. Heine, S. Verma and R. Banerjee, *Chem. Sci.*, 2015, **6**, 3931–3939.
36 N. Kwon, Y. Hu and J. Yoon, *ACS Omega*, 2018, **3**, 13731–13751.
37 M. A. H. Khan, M. V. Rao and Q. Li, *Sensors*, 2019, **19**, 905–944.
38 R. B. Onyancha, K. E. Ukhurebor, U. O. Aigbe, O. A. Osibote, H. S. Kusuma, H. Darmokoesoemo and V. A. Balogun, *Sens. Bio-Sens. Res.*, 2021, **34**, 100463.
39 M. Safaei, M. M. Foroughi, N. Ebrahimpoor, S. Jahani, A. Omidi and M. Khatami, *TrAC, Trends Anal. Chem.*, 2019, **118**, 401–425.
40 C. S. Hawes, K. Byrne, W. Schmitt and T. Gunnlaugsson, *Inorg. Chem.*, 2016, **55**, 11570–11582.
41 H. Furukawa, K. E. Cordova, M. O'Keeffe and O. M. Yaghi, *Science*, 2013, **341**, 1230444.
42 F. David, *Metal–Organic Frameworks: Applications from Catalysis to Gas Storage*, Wiley-VCH, Weinheim, 2011, p. 414.
43 Y. Cui, Y. Yue, G. Qian and B. Chen, *Chem. Rev.*, 2012, **112**, 1126–1162.
44 P. R. Lakshmi, P. Nanjan, S. Kannan and S. Shanmugaraju, *Coord. Chem. Rev.*, 2021, **435**, 213793–213820.
45 B. Zhang, P.-Y. Guo, L.-N. Ma, B. Liu, L. Hou and Y.-Y. Wang, *Inorg. Chem.*, 2020, **59**, 5231–5239.
46 A. Kirchon, L. Feng, H. F. Drake, E. A. Joseph and H.-C. Zhou, *Chem. Soc. Rev.*, 2018, **47**, 8611–8638.
47 N. B. Shustova, A. F. Cozzolino, S. Reineke, M. Baldo and M. Dincă, *J. Am. Chem. Soc.*, 2013, **135**, 13326–13329.
48 Y.-P. Li, S.-N. Li, Y.-C. Jiang, M.-C. Hu and Q.-G. Zhai, *Chem. Commun.*, 2018, **54**, 9789–9792.
49 B. Zhu, Y. Jin, J. Chu, M. Zuo and S. Cui, *RSC Adv.*, 2022, **12**, 6951–6957.
50 D. I. Pavlov, T. S. Sukhikh, A. A. Ryadun, V. V. Matveevskaya, K. A. Kovalenko, E. Benassi, V. P. Fedin and A. S. Potapov, *J. Mater. Chem. C*, 2022, **10**, 5567–5575.
51 A. J. Savyasachi, O. Kotova, S. Shanmugaraju, S. J. Bradberry, G. M. Ó'Máille and T. Gunnlaugsson, *Chem*, 2017, **3**, 764–811.
52 S. Roy and T. K. Maji, *Chem. Commun.*, 2022, **58**, 4149–4167.
53 Y. Cheng, Q. Feng, M. Yin, C. Wang and Y. Zhou, *Tetrahedron Lett.*, 2016, **57**, 3814–3818.
54 Y. Xu, X. Zhang, W. Zhang, X. Liu and Q. Liu, *J. Photochem. Photobiol., A*, 2021, **404**, 112901.
55 S. Shanmugaraju, D. Umadevi, A. J. Savyasachi, K. Byrne, M. Ruether, W. Schmitt, G. W. Watson and T. Gunnlaugsson, *J. Mater. Chem. A*, 2017, **5**, 25014–25024.
56 S. Wang, H. Li, H. Huang, X. Cao, X. Chen and D. Cao, *Chem. Soc. Rev.*, 2022, **51**, 2031–2080.
57 T. Skorjanc, D. Shetty and M. Valant, *ACS Sens.*, 2021, **6**, 1461–1481.
58 Z. Meng and K. A. Mirica, *Chem. Soc. Rev.*, 2021, **50**, 13498–13558.

59 S. Zhang, D. Liu and G. Wang, *Molecules*, 2022, **27**, 2586.
60 F.-Z. Cui, J.-J. Xie, S.-Y. Jiang, S.-X. Gan, D.-L. Ma, R.-R. Liang, G.-F. Jiang and X. Zhao, *Chem. Commun.*, 2019, **55**, 4550–4553.
61 K. Prakash and D. T. Masram, *Dalton Trans.*, 2020, **49**, 1007–1010.
62 K. Prakash and D. T. Masram, *J. Mater. Chem. C*, 2020, **8**, 9201–9204.
63 N. Xu, R.-L. Wang, D.-P. Li, Z.-Y. Zhou, T. Zhang, Y.-Z. Xie and Z.-M. Su, *New J. Chem.*, 2018, **42**, 13367–13374.
64 Y. Takagai, Y. Nojiri, T. Takase, W. L. Hinze, M. Butsugan and S. Igarashi, *Analyst*, 2010, **135**, 1417–1425.
65 S. Dalapati, E. Jin, M. Addicoat, T. Heine and D. Jiang, *J. Am. Chem. Soc.*, 2016, **138**, 5797–5800.
66 B. Gole, S. Shanmugaraju, A. K. Bar and P. S. Mukherjee, *Chem. Commun.*, 2011, **47**, 10046–10048.
67 S. Shanmugaraju, H. Jadhav, R. Karthik and P. S. Mukherjee, *RSC Adv.*, 2013, **3**, 4940–4950.
68 A. V. Raveendran, P. A. Sankeerthana, A. Jayaraj and P. C. A. Swamy, *Results Chem.*, 2022, **4**, 100297–100351.
69 S. Mukherjee and P. Thilagar, *J. Mater. Chem. C*, 2013, **1**, 4691–4698.
70 H. Liu, J. Mack, Q. Guo, H. Lu, N. Kobayashi and Z. Shen, *Chem. Commun.*, 2011, **47**, 12092–12094.
71 J. Kim, S.-H. Lim, Y. Yoon, T. D. Thangadurai and S. Yoon, *Tetrahedron Lett.*, 2011, **52**, 2645–2648.
72 K. P. McDonald, B. Qiao, E. B. Twum, S. Lee, P. J. Gamache, C.-H. Chen, Y. Yi and A. H. Flood, *Chem. Commun.*, 2014, **50**, 13285–13288.
73 J. M. Mahoney, A. M. Beatty and B. D. Smith, *J. Am. Chem. Soc.*, 2001, **123**, 5847–5848.
74 T. M. Jonah, L. Mathivathanan, A. N. Morozov, A. M. Mebel, R. G. Raptis and K. Kavallieratos, *New J. Chem.*, 2017, **41**, 14835–14838.
75 B. J. Müller, N. Steinmann, S. M. Borisov and I. Klimant, *Sens. Actuators, B*, 2018, **255**, 1897–1901.
76 R. Chakrabarty, P. S. Mukherjee and P. J. Stang, *Chem. Rev.*, 2011, **111**, 6810–6918.
77 T. Han, W. Wei, J. Yuan, Y. Duan, Y. Li, L. Hu and Y. Dong, *Talanta*, 2016, **150**, 104–112.
78 L. Wu, A. C. Sedgwick, X. Sun, S. D. Bull, X.-P. He and T. D. James, *Acc. Chem. Res.*, 2019, **52**, 2582–2597.
79 J. Ohata, K. J. Bruemmer and C. J. Chang, *Acc. Chem. Res.*, 2019, **52**, 2841–2848.
80 M. Maierhofer, V. Rieger and T. Mayr, *Anal. Bioanal. Chem.*, 2020, **412**, 7559–7567.
81 M. Strobl, A. Walcher, T. Mayr, I. Klimant and S. M. Borisov, *Anal. Chem.*, 2017, **89**, 2859–2865.
82 H. D. Duong and J. Il Rhee, *Sens. Actuators, B*, 2014, **190**, 768–774.
83 E. Zhang, X. Hou, H. Yang, Y. Zou and P. Ju, *Anal. Methods*, 2020, **12**, 1744–1751.